

EigenLoRAX: Recycling Adapters to Find Principal Subspaces for Resource-Efficient Adaptation and Inference

Prakhar Kaushik*¹ Ankit Vaidya*¹ Shravan Chaudhari¹ Alan Yuille¹

Abstract

The rapid growth of large models has raised concerns about their environmental impact and equity in accessibility due to significant computational costs. Low-Rank Adapters (LoRA) offer a lightweight solution for finetuning large models, resulting in an abundance of publicly available adapters tailored to diverse domains. We ask: Can these pretrained adapters be leveraged to further streamline adaptation to new tasks while addressing these challenges? We introduce EigenLoRAX, a parameter-efficient finetuning method that recycles existing adapters to create a principal subspace aligned with their shared domain knowledge which can be further augmented with orthogonal basis vectors in low-resource scenarios. This enables rapid adaptation to new tasks by learning only lightweight coefficients on the principal components of the subspace - eliminating the need to finetune entire adapters. EigenLoRAX requires significantly fewer parameters and memory, improving efficiency for both training and inference. Our method demonstrates strong performance across diverse domains and tasks, offering a scalable for edge-based applications, personalization, and equitable deployment of large models in resource-constrained environments.

1. Introduction

Recent advancements in natural language processing (Touvron et al., 2023) and computer vision (Rombach et al., 2021) have driven the rise of large-scale models with billions of parameters. However, the size and complexity of these models not only make it impractical for most researchers to train or fine-tune them on downstream tasks but also contribute significantly to their carbon footprint, raising concerns about environmental sustainability. To

*Equal contribution ¹Department of Computer Science, Johns Hopkins University, Baltimore, USA. Correspondence to: Prakhar Kaushik <pkaushi1@jh.edu>.

Preprint, 2025.

address these challenges, there has been growing interest in parameter-efficient finetuning (PEFT) methods, such as adapters (Houlsby et al., 2019; Chen et al., 2022; Luo et al., 2023), low rank adaptation (LoRA) methods (Hu et al., 2021; Kopiczko et al., 2023; Liu et al., 2024), prompt-based methods (Lester et al., 2021; Razdaibiedina et al., 2023; Fischer et al., 2024).

LoRA and its follow-up works (Meng et al., 2024; Liu et al., 2024) have gained significant attention for their simplicity. This has fueled the proliferation of thousands of low-rank adapters within the growing open-source community. Given that these adapters are underutilized, an important question arises: Can we recycle the information contained in them to improve the efficiency of subsequent tasks? Recent work has shown that weight updates in deep neural networks occur within low-dimensional invariant subspaces (Kwon et al., 2024), aligning with the universality hypothesis that neural network behavior and learned representations often reside in shared, structured subspaces (Chughtai et al., 2023; Guth & Ménard, 2024). This suggests that LoRA adapters may similarly share a *principal subspace* that can be reused, eliminating the need to rediscover it during the training of new adapters.

We introduce **EigenLoRAX**, a parameter-efficient finetuning (PEFT) method that leverages this insight by decomposing the weights of a set of trained adapters into principal components, identifying a compact, information-dense subspace. EigenLoRAX reduces the number of learnable parameters by up to $100\times$ compared to LoRA, accelerates optimization by up to $2\times$ for new adapters, and enables more memory-efficient inference with multiple task adapters, particularly benefiting edge devices (Liu et al., 2022). Additionally, in low-resource domains, we demonstrate that EigenLoRAX can be further enhanced by augmenting the principal subspace with random components, orthogonalized with respect to the existing subspace, preserving its efficiency while retaining performance.

Furthermore, we provide an initial theoretical analysis of EigenLoRAX. Our experiments across a wide range of vision and language tasks demonstrate its versatility and effectiveness, reinforcing the potential of shared subspaces in neural network adaptation.

Figure 1 provides an overview of our method. We introduce **EigenLoRAX** (ELoRAX), which recycles pretrained adapters by identifying a shared *task-invariant* weight subspace. We hypothesize (and validate experimentally) that task-specific weights lie within this subspace, allowing for more efficient training with fewer parameters. This reduces memory footprint and enhances inference efficiency by enabling simultaneous serving of multiple adapters. EigenLoRAX is among the first to recycle pretrained adapters, replacing many while improving further training efficiency. Our key contributions are as follows:

- **(Training):** EigenLoRAX uses up to **100× fewer parameters than LoRA** and converges up to **2× faster** than comparable methods, achieving similar or better performance.
- **(Inference):** EigenLoRAX enhances **memory efficiency during inference** by approximately **18×** on multiple tasks, reducing the number of switchable parameters between tasks.
- **(Applicability):** We empirically demonstrate the effectiveness of EigenLoRAX across a wide range, including text and image data, validating the existence of shared principal subspaces across modalities. It also retains performance in **zero-shot** and **low resource** scenarios.
- **(Scaling):** EigenLoRAX can be scaled up to recycle hundreds of underutilized pretrained adapters.

2. Related Works

Low-Rank Adaptation refers to modeling neural network weight updates as a function of low-rank matrices instead of training the entire weight matrix. This is a well-established line of research starting from Burer-Monteiro factorization (Burer & Monteiro, 2003), with a recent resurgence by Hu et al. (2021) (LoRA), who used it as a technique to finetune LLMs; and other related variants (Ma et al., 2024; Chi et al., 2019; Kwon et al., 2024). However, with rapid growth in the scale of models, Low-Rank Adaptation has also become relatively expensive; for example, LoRA with a rank of 16 on GPT-3 (Brown et al., 2020) requires 75.5 million parameters. Consequently, more efficient low-rank fine-tuning methods are being developed. Mixture of experts models (Huang et al., 2023; Wu et al., 2024; Diao et al., 2023; Zhong et al., 2024; Zhou et al., 2018) have been proposed as a method to adapt to new domains using a mixture of low-rank modules. But these approaches typically require a substantial number of high-quality adapters to work efficiently (Ku et al., 2024), which can significantly increase the model memory requirements (Zhou et al., 2022). Furthermore, complex gating or weighting mechanisms utilized

with these models can exhibit training instability (Zoph et al., 2022).

Recent methods have aimed to learn better subspaces for low-rank optimization, primarily by decomposing model weights into singular vectors for improved training. Meng et al. (2024) demonstrate that initializing LoRA with singular vectors is superior to random initialization, while Sharma et al. (2023) find that removing minor singular components enhances robustness. Using randomly initialized principal components (Kopczko et al., 2023) or weight matrices (Koohpayegani et al., 2024) has also been explored to reduce the number of trainable parameters. However, as shown in Section 4, random initialized subspaces may not be very useful. This is intuitive as the random subspace may not have an overlap with domain-specific principal subspaces. On the other hand, EigenLoRAX uses trained adapters to extract a *principal subspace* suitable for a given domain of tasks resulting in a better subspace initialization than and parameter efficiency. Given our focus on resource and computation efficiency in this work, we focus primarily on LoRA (Hu et al., 2021) as our main baseline, but EigenLoRAX can be used with any PEFT method like (Liu et al., 2024; Zhang et al., 2023) where task-specific weights can be analyzed together.

3. Method

In this section, we describe the theoretical motivation and the algorithm of our method, with a discussion on the hyperparameters and quantification of practical benefits. Note that we use the terms EigenLoRA, EigenLoRAX, ELoRA and ELoRAX interchangeably.

3.1. Theoretical Motivation

Let $W \in \mathbb{R}^{m \times n}$ be a matrix representing a linear transformation between the vector spaces \mathbb{R}^m and \mathbb{R}^n . When W is of full rank, meaning $\text{rank}(W) = \min(m, n)$, it is capable of expressing the entire space of possible linear mappings between these dimensions. However, as the rank of W increases, modifying it to accommodate new tasks becomes computationally expensive and increasingly complex. To mitigate this challenge in fine-tuning large models, LoRA introduces a decomposition of W into two low-rank matrices, $B \in \mathbb{R}^{m \times r}$ and $A \in \mathbb{R}^{r \times n}$, where $r \ll \min(m, n)$. This factorization ensures that the product BA retains the original dimensions of W while having a significantly reduced rank. That is, $BA \in \mathbb{R}^{m \times n}$, with $\text{rank}(BA) \leq r$. As a result, although the transformation defined by BA maps from \mathbb{R}^m to \mathbb{R}^n , it does not span the full space of such mappings due to its constrained rank. By focusing on learning only the most essential updates within a low-dimensional subspace, LoRA provides a parameter-efficient mechanism for model adaptation. The number of parameters in this adaptation

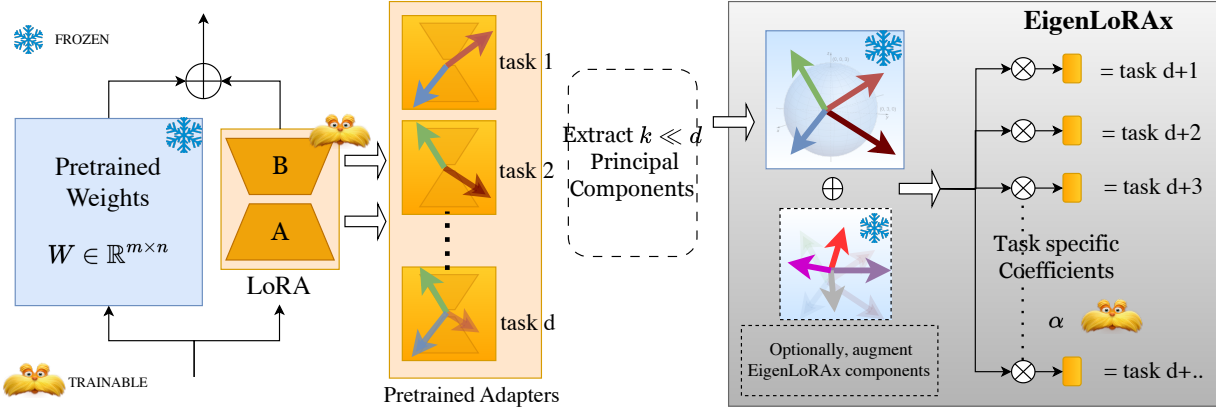


Figure 1: LoRA uses low-rank matrices for task-specific finetuning. We observe that LoRA adapters share a principal subspace across task domains. By recycling pretrained adapters, we extract *task-invariant* principal components, enabling efficient representation of both existing and future LoRAs using compact *task-specific* coefficients. This improves training speed, parameter efficiency, and memory usage. In low-resource settings, where pretrained adapters are scarce, we augment the subspace with randomly initialized components, ensuring orthogonality via the Gram-Schmidt process, ensuring they complement the extracted subspace without redundancy.

framework is given by $m \cdot r + r \cdot n$, which is substantially smaller than the full parameter count $m \cdot n$, making it a computationally viable alternative for fine-tuning large-scale models.

Many downstream adapters have been observed to converge toward a shared set of key directions in their parameter space (Meng et al., 2024; Liu et al., 2024), suggesting the existence of a *principal subspace* underlying diverse tasks. We hypothesize that LoRA adapters leverage such subspaces, enabling task-specific adaptations within a lower-dimensional structure rather than the full weight space. This not only reduces computational overhead but also reinforces the idea that task-relevant transformations reside within a compact, reusable subspace. To formalize this, we first define a space of tasks representable by linear transformation matrices, providing a foundation for analyzing the role of shared principal subspaces in model adaptation.

Definition 3.1 (Linear Transformation Tasks). We define a task domain \mathcal{T}_d as set of d linear tasks, $\mathcal{T}_d = \{t \mid \mathcal{X}_t \in \mathbb{R}^m \rightarrow \mathcal{Y}_t \in \mathbb{R}^n\}$ where for each task $t \in \mathcal{T}_d$, $\exists W_t^* \in \mathbb{R}^{m \times n}$ such that $Y = W_t^* X + \epsilon_t \forall X \in \mathcal{X}_t, Y \in \mathcal{Y}_t$ where ϵ_t denotes the noise in data distribution.

For a given set of pretrained weights (such as those from a foundation model) $W_0 \in \mathbb{R}^{m \times n}$, LoRA weights BA at any layer modify the output as $W_0 X + BAX + \epsilon_t$, allowing the model to adapt to the new task and converge toward the optimal solution W_t^* . The key here is that only B and A weights are updated during finetuning. Without loss of generality, assume $r \ll n$ and let the true transformation matrix $W_t^* \in \mathbb{R}^{r \times n}$ be interpreted as r n -dimensional vectors: $\mathbf{w}_t^{*1}, \dots, \mathbf{w}_t^{*r} \in \mathbb{R}^n$. Finding LoRA weights is equivalent to finding sets of these r vectors in \mathbb{R}^n .

Definition 3.2 (Set of LoRA weights). We define the weights of a LoRA adapted for task t as $B_t A_t$. Both B_t and A_t will have their own individual subspaces. For the purpose of the analysis we will consider a generic task specific weight matrix $W_t \in \mathbb{R}^{m \times n}$ adapted to task t such that $n < m$ and its rank $r < n$. The analysis, however, is valid for both B_t and A_t . Now can define a set of LoRAs as stacked (along columns) weight matrices $\hat{W} = \{W_t\}$ each adapted for a task $t \in \mathcal{T}_d$ and a training set $\mathcal{S}_t = \{\{x_i, y_i\} \mid x_i \in \mathcal{X}_t, y_i \in \mathcal{Y}_t\}_{i=1}^{s_t}$ where $s_t = |\mathcal{S}_t|$ and $\mathcal{X}_t \times \mathcal{Y}_t$ are distributed according to some unknown Gaussian distribution with mean $\bar{\mathcal{X}}_t$ and $\|X\|_F \leq M$ for some constant $M > 0$. Each weight matrix can have different ranks and the following method and analysis will still hold, however, for brevity we assume all weight matrices stacked in \hat{W} to have the same rank r .

Definition 3.3 (Subspace spanned by LoRAs from a task domain \mathcal{T}_d). We define the subspace of weights $\mathcal{Z}_d = \{C\hat{W} \mid C \in \mathbb{R}^{m \times m}\}$ spanned within $\mathbb{R}^{m \times n}$.

Using Singular Value Decomposition (SVD) or Principal Component Analysis (PCA for a zero-centered \hat{W}), we can obtain $\hat{W} = U\Sigma V^T$. We then represent top K right singular vectors of \hat{W} (or top K principal components if \hat{W} is zero-centered) as $\mathcal{V}_K^T \in \mathbb{R}^{K \times n} = \{\mathcal{V}_k^T \in \mathbb{R}^{1 \times n}\}_{k=1}^K$.

Definition 3.4 (Principal Subspace of LoRAs finetuned in domain \mathcal{T}_d). We define the principal subspace of weights for a task domain \mathcal{T}_d as $\mathcal{Z}_d^K = \{\alpha \mathcal{V}_K^T \mid \alpha \in \mathbb{R}^{m \times K}\}$ spanned by top K principal components of the LoRAs within $\mathbb{R}^{m \times n}$.

Next, we introduce the idea of defining a new related task t_{d+1} .

Definition 3.5 (New related task t_{d+1}). . . A new linear

task t_{d+1} with true solution W^* is said to be related if it is spanned by the basis of \hat{W} i.e. $W^* = C\hat{W}$ and it holds that $\|W^* - \alpha_{d+1}^* \mathcal{V}_K^T\|_F^2 \leq \|W^* - \alpha_{d+1} \mathcal{V}_K^T\|_F^2$ for all rank K linear transformation matrices α_{d+1} and $\|W^* - \alpha_{d+1}^* \mathcal{V}_K^T\|_F^2 \leq \|C\|_2^2 \sum_{i=K+1}^n \sigma_i^2$ where σ_i 's are singular values of \hat{W} . For such a task, we learn coefficients of K principal components $\alpha_{d+1} \in \mathbb{R}^{m \times K}$ resulting in EigenLoRAX weights $W_{\mathcal{E}} = \alpha_{d+1} \mathcal{V}_K^T$.

Definition 3.5 establishes a bound over the relatedness of a new task with those in the known task domain \mathcal{T}_d . If the true solution of the new task lies majorly in the principal subspace of \mathcal{T}_d i.e. has major principal components (PCs) within the top K principal components of \hat{W} with some finite bound on the misalignment along the PCs orthogonal to the top K PCs of \hat{W} , then we can ideally quantify the relation between a new task and a task domain. Any task that has its true solution within a subspace defined by the PCs orthogonal to the top K PCs of \hat{W} is not as closely related as a task with its solution completely or majorly within the principal subspace. A task that has its solution completely orthogonal to all the PCs of \hat{W} is completely unrelated and is not the main focus of this study.

Next, we present an algorithm to find the principal subspace of the trained adapters and our experiments in Section 4.

Algorithm 1 EigenLoRAX PCs Calculation

Input: LoRA matrices $\{W_t \in \mathbb{R}^{m \times n}\}_{t=1}^d$, number of PC (K), number of pseudo-PC (P)
Output: EigenLoRAX PCs \mathcal{V}_K^T

$$\hat{W} = [W_1 \in \mathbb{R}^{m \times n} \quad \dots \quad W_d \in \mathbb{R}^{m \times n}], \{\text{Stack LoRA matrices}\}$$

Compute the mean of each feature: $\bar{W} = \frac{1}{n} \sum_{i=1}^n W_i$

Subtract the mean: $\hat{W}_c = \hat{W} - \bar{W}$

Perform SVD: $\hat{W}_c = U \Sigma V^T$

Extract the top K principal components

Select the first K columns of V : $\mathcal{V}_K = V[:, 1 : K]$

Optionally, augment the subspace with P pseudo-PCs
for $p = 1$ to P **do**

- Sample a random vector $v_p \sim \mathcal{N}(0, I_n)$ {Sample from a normal distribution}
- Orthogonalize v_p against all PCs in \mathcal{V}_K using Gram-Schmidt:
- for** $i = 1$ to $K + p - 1$ **do**

 - $v_p = v_p - \frac{v_p^T \mathcal{V}_K[:, i]}{\|\mathcal{V}_K[:, i]\|^2} \mathcal{V}_K[:, i]$

- end for**
- Normalize v_p : $v_p = \frac{v_p}{\|v_p\|}$
- Append v_p to \mathcal{V}_K if v_p is not a null vector
- $K = K + 1$

end for

return \mathcal{V}_K, μ

3.2. Algorithm

Assume we have N LoRA adapters, each consisting of a set of A, B matrix pairs for every layer, trained on various tasks within a domain \mathcal{T}_d for a given base pretrained model. Algorithm 1 computes a list of top K principal components—referred to as EigenLoRAX PCs—that define an initial principal subspace for this domain. To construct this subspace, the algorithm aggregates LoRA matrices across tasks for each layer, separately for A and B matrices (though it can also be applied to the product BA). Each LoRA matrix, having rank r , is treated as a list of vectors, and a decomposition is performed on this stacked set of vectors. The most significant components extracted from this process serve as a basis for the principal subspace, providing an efficient representation that can be linearly combined to approximate the original LoRA weight matrices. We illustrate our algorithm using generic weight matrices W_t , where each W_t represents a single A or B matrix from a single layer of the neural network. In practice, this procedure is applied to all relevant layers.

Since real-world scenarios often involve low-resource domains with limited availability of LoRA adapters, we extend our subspace by introducing additional pseudo-PCs. Specifically, we sample random vectors of the same dimension as each PC and orthogonalize them with respect to all existing PCs. This process can be iterated to generate more pseudo-PCs, thereby augmenting the principal subspace. As empirically shown in Table 3, this augmentation strategy significantly outperforms naive random selection of PCs for subspace expansion.

Learning new tasks Having extracted a set of PCs (including pseudo-PCs, if needed), $\mathcal{V}_K \in \mathbb{R}^{K \times n} = \{\mathcal{V}_K \in \mathbb{R}^{1 \times n}\}_{k=1}^K$, we can approximate a given (LoRA) weight matrix by minimizing $\|W - \alpha \mathcal{V}_K^T\|_F$ where α are linear coefficients Section 3.1. In fact, we can analytically compute of the given LoRA matrices by calculating the linear coefficients which minimizes the above objective. For new tasks however, for which we do not have a LoRA matrix, we freeze the EigenLoRAX PCs and randomly initialize the α s. The forward pass in layer is calculated as

$$h = W_0 x + \left[\alpha_B^T \mathcal{V}_B \alpha_A^T \mathcal{V}_A(x) \right]. \quad (1)$$

Here, W_0 are the pre-trained base model weights and $\mathcal{V}_B, \mathcal{V}_A$ are EigenLoRAX PCs that remain fixed during training. The corresponding α_B and α_A are learned. This reduces the number of learnable parameters from $O(rn)$ to $O(rK)$, by a factor of $\frac{n}{K}$ (assuming rank r to be fixed, which could also be changed).

Using the definitions 3.1, 3.2, 3.5, 3.4 and 3.3 we state the following theorem;

Theorem 3.6. For a task t_{d+1} , we assume a hypothesis $h \in \mathcal{H}_{W_{d+1}}$ expressed as $h(W_{d+1}, X) = W_{d+1}X + W_0X + b$ where W_{d+1} has rank m , b is some constant and W_0 represents weights of a pretrained foundation model that is frozen during finetuning and X, Y are sampled from $\mathcal{X}_t, \mathcal{Y}_t$ respectively. We have $h^* \in \mathcal{H}_{W_{\mathcal{E}}}, h^* \in \mathcal{H}_W$ such that $h^*(W_{\mathcal{E}}, X) = \alpha_{d+1}\mathcal{V}_K^T X + W_0X + b$ where $W_{\mathcal{E}}$ has rank K and $h^*(W^*, X) = C\hat{W}X + W_0X + b$ where $h^*(W_{d+1}, X) = Y$ is the true solution for task t_{d+1} . For a Lipschitz continuous loss ($\ell_{\mathcal{S}_t}^F(h_W)$) that is strong convex within the principal subspace defined by principal components \mathcal{V}_K^T with Lipschitz constant (L), the risk can be written as $R_{\mathcal{S}_t}^F(h_W) = E[\ell_{\mathcal{S}_t}^F(h_W)]$, and using Rademacher complexity bounds we can say with probability at least $1 - 4\delta$ for some $\delta > 0$,

$$\|W^* - W_{d+1}\|_F^2 \leq C_1 \cdot \left(\frac{\sqrt{m}}{\sqrt{s_t}} \right) + C_2 \quad (2)$$

$$\|\alpha_{d+1}^* \mathcal{V}_K^T - W_{\mathcal{E}}\|_F^2 \leq C_1 \cdot \left(\frac{\sqrt{K}}{\sqrt{s_t}} \right) + \|C\|_2^2 \sum_{i=K+1}^{nd} \sigma_i^2 + C_2 \quad (3)$$

where σ_i are singular values of \hat{W} , C is some constant such that $W^* = C\hat{W}$ and C_1, C_2 are some constants.

Proof. The derivation is straightforward, we can write the difference in risks for $h^{\mathcal{E}}$ and h^* as

$$R_{\mathcal{S}_t}^F(h^{\mathcal{E}}) - R_{\mathcal{S}_t}^F(h^*) = \mathbb{E}_{\mathcal{S}_t} [\ell_{\mathcal{S}_t}^F(h^{\mathcal{E}}) - \ell_{\mathcal{S}_t}^F(h^*)]$$

By definition of strong convex loss function for some constant $\mu \geq 0$,

$$\mathbb{E}_{\mathcal{S}_t} [\ell_{\mathcal{S}_t}^F(h^{\mathcal{E}}) - \ell_{\mathcal{S}_t}^F(h^*)] \geq \frac{\mu}{2} \|W_{\mathcal{E}} - W^*\|_F^2$$

We also know from generalization error bounds using Rademacher Complexity from (Bartlett & Mendelson, 2003) that with probability at least $1 - 2\delta$,

$$|R_{\mathcal{S}_t}^F(h^{\mathcal{E}}) - \hat{R}_{\mathcal{S}_t}^F(h^{\mathcal{E}})| \leq \frac{\mathcal{R}_{s_t}(\mathcal{H}_{W_{\mathcal{E}}})}{2} + \sqrt{\frac{\ln(1/\delta)}{2s_t}}$$

We can rewrite risk as

$$\begin{aligned} R_{\mathcal{S}_t}^F(h^*) - R_{\mathcal{S}_t}^F(h^{\mathcal{E}}) &= R_{\mathcal{S}_t}^F(h^*) - \hat{R}_{\mathcal{S}_t}^F(h^*) - R_{\mathcal{S}_t}^F(h^{\mathcal{E}}) \\ &\quad + \hat{R}_{\mathcal{S}_t}^F(h^{\mathcal{E}}) + \hat{R}_{\mathcal{S}_t}^F(h^*) - \hat{R}_{\mathcal{S}_t}^F(h^{\mathcal{E}}) \end{aligned}$$

Since we know by definition of h^* that $\hat{R}_{\mathcal{S}_t}^F(h^*) \leq \hat{R}_{\mathcal{S}_t}^F(h^{\mathcal{E}})$, we can say

$$\begin{aligned} R_{\mathcal{S}_t}^F(h^*) - R_{\mathcal{S}_t}^F(h^{\mathcal{E}}) &\leq R_{\mathcal{S}_t}^F(h^*) - \hat{R}_{\mathcal{S}_t}^F(h^*) \\ &\quad - R_{\mathcal{S}_t}^F(h^{\mathcal{E}}) + \hat{R}_{\mathcal{S}_t}^F(h^{\mathcal{E}}) \end{aligned}$$

Then we take a union bound to conclude that with probability at least $1 - 4\delta$,

$$R_{\mathcal{S}_t}^F(h^*) - R_{\mathcal{S}_t}^F(h^{\mathcal{E}}) \leq \mathcal{R}_{s_t}(\mathcal{H}_{W_{\mathcal{E}}}) + \sqrt{\frac{2 \ln(1/\delta)}{s_t}}$$

Hence, we can also say that with probability at least $1 - 4\delta$,

$$\frac{\mu}{2} \|W^* - W_{\mathcal{E}}\|_F^2 \leq \mathcal{R}_{s_t}(\mathcal{H}_{W_{\mathcal{E}}}) + \sqrt{\frac{2 \ln(1/\delta)}{s_t}} \quad (4)$$

The Rademacher complexity of a low-rank weight matrix class $\mathcal{H}_{W_{\mathcal{E}}}$ with rank K can be directly bounded using results from (Bartlett & Mendelson, 2003) as

$$\begin{aligned} \mathcal{R}_{s_t}(\mathcal{H}_{W_{\mathcal{E}}}) &= \mathcal{O}\left(\frac{\sqrt{K} \|W_{\mathcal{E}}\|_F}{\sqrt{s_t}}\right) \\ &= C_1 \cdot \left(\frac{\sqrt{K} \|W_{\mathcal{E}}\|_F}{\sqrt{s_t}} \right) + C_2 \end{aligned}$$

For a normalised $\|W_{\mathcal{E}}\|$ is usually bounded Hence,

$$\|W^* - W_{\mathcal{E}}\|_F^2 \leq C_1 \cdot \left(\frac{\sqrt{K}}{\sqrt{s_t}} \right) + C_2 \quad (5)$$

Similarly, we can also say for W_{d+1} that

$$\|W^* - W_{d+1}\|_F^2 \leq C_1 \cdot \left(\frac{\sqrt{m}}{\sqrt{s_t}} \right) + C_2 \quad (6)$$

This proves 2. Now to further prove 3, we use properties of Frobenius norm,

$$\|W_{\mathcal{E}} - \alpha_{d+1}^* \mathcal{V}_K^T\|_F^2 - \|W^* - \alpha_{d+1}^* \mathcal{V}_K^T\|_F^2 \leq \|W_{\mathcal{E}} - W^*\|_F^2$$

Then following from the definition of W^* , we can say that,

$$\|W_{\mathcal{E}} - \alpha_{d+1}^* \mathcal{V}_K^T\|_F^2 - \|C\|_2^2 \sum_{i=K+1}^{nd} \sigma_i^2 \leq \|W_{\mathcal{E}} - W^*\|_F^2$$

Finally, using the Rademacher complexity bound we provided earlier, we can say that with probability at least $1 - 4\delta$

$$\begin{aligned} \|\alpha_{d+1}^* \mathcal{V}_K^T - W_{\mathcal{E}}\|_F^2 &\leq \|W^* - W_{\mathcal{E}}\|_F^2 \\ &\leq C_1 \cdot \left(\frac{\sqrt{K}}{\sqrt{s_t}} \right) + \|C\|_2^2 \sum_{i=K+1}^{nd} \sigma_i^2 + C_2 \end{aligned}$$

We can just rewrite $W_{\mathcal{E}} = \alpha_{d+1}^* \mathcal{V}_K^T$ and get the same bound as above for $\|\alpha_{d+1}^* - \alpha_{d+1}\|_F^2$. We can similarly obtain the upper bound for 3

This concludes the proof. \square

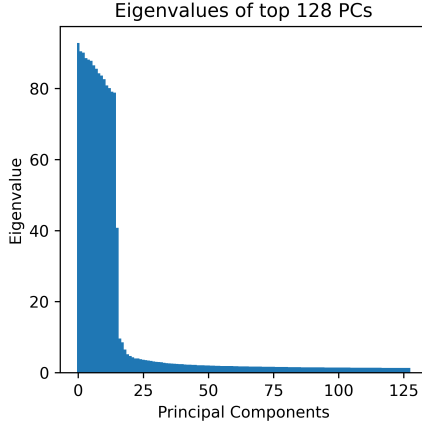


Figure 2: The top 16 components are most information dense (A matrices from layer 1, Lots of LoRAs, see Section 4.3).

Theorem 3.6 provides an upper bound on the Frobenius norm of the difference between W_{d+1} or $W_{\mathcal{E}}$ and the optimal solution W^* . 3 provides a tighter upper bound on the norm of the difference when task t_{d+1} majorly lies in the principal subspace. The extent to which task t_{d+1} lies in the principle subspace is captured by the second term involving the sum of squared truncated singular values \hat{W} . Hence, if the task completely or majorly lie in the principal subspace, then the first term (sqrt(rank)) will dominate the upper bound. Hence, if $\text{rank}W_{d+1} \geq K$, then we can see that the upper bound in 3 will be tighter than 2 when the task lies majorly in the principal subspace. Similarly, when $m \leq K$, the upper bound on the difference norm will be tighter for W_{d+1} than $W_{\mathcal{E}}$. When W^* has a significant alignment or projection along the singular vectors orthogonal to the ones with top K singular values, then the second term in 2 comes into picture and it becomes difficult to directly compare the bounds in 2 and 3. However, if majority of the variance of W^* is along the singular vectors orthogonal to the top K components, it follows that $W_{\mathcal{E}}$ will never be able to achieve convergence while W_{d+1} . In contrast, W_{d+1} could perform significantly better, as it is not restricted to learning only along the top K principal components of \hat{W} .

How to choose optimal number of PCs K The hyperparameter K , which determines the number of top PC, can be viewed as a function of task domain complexity—simpler domains require a smaller K , while more complex domains benefit from a larger K . In practice, we determine K based on empirical observations (Appendix B), evaluating performance across different values. Additionally, we can leverage established techniques from literature, such as explained variance and singular value thresholds (Gavish & Donoho, 2014). As illustrated in Figure 2, most of the relevant information is often concentrated in a few top EigenLoRAX PCs,

providing a practical criterion for selecting K .

Memory Efficiency Our method demonstrates significant memory efficiency across experiments. A single set of EigenLoRAX PCs, combined with lightweight task-specific coefficients, can effectively replace both past and future LoRAs within a task domain. This is particularly advantageous when serving a large number of adapters, where frequent loading and unloading in VRAM incurs high latency, or keeping all adapters in memory demands excessive VRAM. For N LoRAs, the memory footprint is $O(Nrn)$. For EigenLoRAXs, it is $O(Kn + NrK)$. As $r, K \ll n$, EigenLoRAX becomes $\frac{n}{K}$ times more memory efficient asymptotically. This becomes significantly useful for edge devices and large scale user serving AI systems.

4. Experiments and Analysis

In this section, we demonstrate the efficacy and versatility of EigenLoRAX across diverse tasks, modalities, and model architectures, highlighting its individual advantages. EigenLoRAX requires significantly fewer parameters to match or surpass LoRA’s performance (Tables 1, 2) and achieves similar or faster loss convergence (Figure 3), making it a cost-effective alternative to random initialization and other methods (Meng et al., 2024). Additionally, we showcase its memory-efficient inference capabilities with a Stable Diffusion text-to-image generation model (Rombach et al., 2021) (Section 4.4). Notably, EigenLoRAX retains its efficiency even in low-resource scenarios where a large number of LoRAs are unavailable.

Note on Baselines Our focus is on recycling adapter knowledge and improving training and memory efficiency while maintaining performance, not solely on maximizing performance. We compare primarily with LoRA, as EigenLoRAX builds its principal subspace using pretrained LoRA adapters. Using better adapters and optimization could further enhance the subspace and performance.

Due to lack of space, more experiments (3D Object pose estimation) and detailed ablation experiments are presented in Appendix A.

4.1. Image Classification

This simpler task involves related datasets where the LoRAs used to construct EigenLoRAX are well-aligned with the downstream tasks, highlighting its finetuning efficiency.

Setup We evaluate EigenLoRAX using a pretrained Vision Transformer (ViT) (Dosovitskiy et al., 2021) across 3 datasets. Each dataset is partitioned into 5–6 non-overlapping sub-datasets, mimicking continual learning (Kaushik et al., 2021) and federated learning (Shenaj

Table 1: Image classification with Vision Transformer. ZS refers to zero-shot. AUG refers to Augmented for Low-Resource. EigenLoRAX matches or increases performance with drastically fewer number of parameters.

	# TRAIN PARAMS	CIFAR 100	FOOD 101	FLOWERS 102
FULL TRAINING	86M	97.0	96.64	98.82
BASE MODEL	15K	90.07	90.8	80.71
LoRA ($r = 4$)	+147K	93.79	95.73	95.03
LoRA ($r = 1$)	+36K	92.45	91.07	90.14
VeRA	+18K	90.87	91.75	91.25
ELoRAX ^{AUG}	+1K	94.4	95.01	97.5
ELoRAX	+96	94.8	95.14	98.44
ELoRAX ^{ZS}	+0	91.4	92.48	95.7

et al., 2023) setups. As the sub-datasets are derived from the same source, their tasks are more domain-aligned. For EigenLoRAX, we compute principal components (PCs) using all but one LoRA trained on individual sub-datasets (leave-one-out approach, Algorithm 1). The coefficient matrix α for the excluded task is then learned as described in Section 3.2. All methods are finetuned for 10 epochs, with additional details in Appendix A.1.

Parameter Efficiency Table 1 summarizes our experimental results. All models require training the last linear layer (approx. 15K parameters) due to the pre-trained ViT having a different number of categories. For the Base Model, no additional parameters are trained. EigenLoRAX adapts to new sub-datasets using only two principal components (96 additional parameters), enabling it to match or outperform LoRA and VeRA, which use significantly more parameters. We also tested a zero-shot EigenLoRAX (weight initialized randomly within the principal subspace), training only the last layer. This model outperforms the base model with no additional parameters, demonstrating the effectiveness of principal subspace extraction. We also test a low resource scenario (ELoRAX^{AUG}), where only 2 LoRAs are available for extracting the PCs, which are then augmented using random, orthogonal PCs as described in Algorithm 1.

4.2. GLUE Benchmark

Next, we evaluate EigenLoRAX on the General Language Understanding Evaluation (GLUE) benchmark (Wang et al., 2019) datasets using the RoBERTa_{base} model (Liu et al., 2019). We use 6 different tasks: MRPC, SST-2, CoLA, QNLI, RTE and STS-B. Following the setup of VeRA, we omit time-intensive MNLI and QQP tasks, thus avoiding the use of MNLI initialization for MRPC, RTE, and STS-B tasks. In this setting, LoRAs are trained not on sub-datasets but on these different datasets representing a *heterogeneous*

domain setting, where the domain difference may be larger relative to the more domain-aligned setting in Section 4.1. We follow the previous leave-one-out evaluation setup, where EigenLoRAX PCs are calculated using LoRAs of all but one task, and α is learnt for the left-out task. Refer to Appendix A.2 for all hyperparameters and implementation details.

Faster Convergence Our results in Table 2 show that EigenLoRAX ($K = 32$) matches LoRA’s performance with **100× fewer trainable parameters** and outperforms VeRA. EigenLoRAX extracts a useful principal subspace across diverse domains, enabling robust adaptation to new tasks. We also evaluate EigenLoRAX(^{init}) weight initialization speed-up. Unlike PiSSA (Meng et al., 2024), which initializes LoRA matrices with principal directions of pre-trained weights, we randomly initialize weights within our extracted subspace. As shown in Figure 3, EigenLoRAX converges faster than PiSSA and VeRA, and slightly faster than LoRA, highlighting the effectiveness of the principal subspace. VeRA’s poorer performance may stem from sub-optimal random initialization that fails to align with task-critical components. ELoRAX is also more efficient in terms of floating point operations for both forward and backward pass, as shown in Table 14.

Low-Resource Scenario To demonstrate the effectiveness of our subspace augmentation strategy Algorithm 1, we conduct an experiment where EigenLoRAX is initialized with only 1–2 LoRAs. The results are presented in Table 3. We compare our method against augmenting EigenLoRAX with random components (EigenLoRAX+random) and using entirely random components (ELoRAX^{random}). As shown, our augmentation approach significantly outperforms random principal component selection. Interestingly, for MRPC, the base model’s performance is retained. This suggests that the learned LoRA weights may not have influenced the base model, likely because they did not capture relevant information. While we do not provide theoretical guarantees for our principal component augmentation strategy—where randomly sampled vectors are iteratively orthogonalized to the existing EigenLoRAX principal vectors—we hypothesize that this targeted guidance helps prevent redundancy within the subspace. Consequently, it increases the likelihood of capturing the necessary task-relevant components.

4.3. Lots of LoRAs

Finally, we also tested our method in settings where a large number of adapters may be trained on significantly diverse domains. Lots of LoRAs (Brüel-Gabrielsson et al., 2024) is a collection of over 500 adapters of the Mistral-7B-Instruct-v0.2 model (Jiang et al., 2023), trained on a variety of natural instruction tasks (Wang et al., 2022). It represents the realis-

Table 2: GLUE benchmark results. We report Matthew’s correlation for CoLA, Pearson correlation for STS-B, and accuracy for the remaining tasks. In all cases, higher values indicate better performance.

METHOD	# TRAINABLE PARAMETERS	MRPC	SST-2	CoLA	QNLI	RTE	STS-B	AVG.
FULL TRAINING	125M	88.97	91.28	59.81	92.29	79.78	90.89	83.84
PISSA [38]	1.2M	86.52	94.15	61.32	92.15	71.84	90.25	82.70
EIGENLORAX ^{INIT}	1.2M	89.71	93.35	61.58	92.2	74.73	89.56	83.52
LORA ($r = 32$)	1.2M	86.76	94.72	59.56	92.53	77.61	90.81	83.67
VERA ($r = 256$)	25K	75.98	93.23	54.14	89.21	66.78	87.03	77.72
EIGENLORAX	12K	87	94.15	59.81	92.73	77.62	90.58	83.65

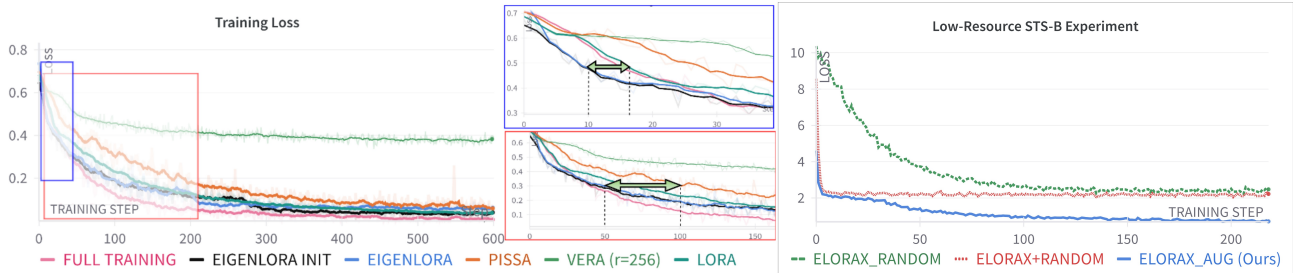


Figure 3: **Fast Convergence and Better Initialization** (left) EigenLoRAX demonstrates faster convergence compared to LoRA and VeRA. EigenLoRAX achieves a speedup of up to $1.5 \times$ against LoRA and up to $2 \times$ compared to PISSA. This experiment was carried out on the CoLA task of the GLUE benchmark.

Table 3: Low-Resource GLUE Subset Results

	# PARAM	MRPC	STS-B
ELORAX ^{RANDOM}	24K	68.38	-0.73
ELORAX+RAND	24K	68.38	0.11
ELORAX ^{AUG}	24K	83.09	85.28

tic setting where we directly use publicly available trained adapters, which may present significant diversity in terms of quality and task domain. As all adapters are accompanied with their respective training datasets, Lots of LoRAs is particularly useful in evaluating EigenLoRAX. The task presents significant diversity and a higher K is necessary to represent this open domain.

Setup We split adapters randomly into two sets (490,5). EigenLoRAX PCs were calculated using the larger “training” set and evaluations were done on the smaller “test” set. We evaluated EigenLoRAX in a zero-shot setting (calculated using the already available adapter weights, no finetuning). The results are shown in Table 4 where we evaluate EigenLoRAX on the 5 tasks from the test set and also on 5 tasks from the training set to check for catastrophic forgetting or concept drift from scaling. The first 5 tasks are randomly sampled from the training set. **EigenLoRAX** nearly

matches LoRA with $12 - 95 \times$ fewer parameters. EigenLoRAX recovers upto 88% of LoRA’s performance even in a zero-shot setting at such a large scale. The performance of EigenLoRAX can be improved by fine-tuning the EigenLoRAX adapters. In this setting we use randomized SVD in order to speed up the calculation of the PCs. We believe this leads to some degradation in performance as there randomized methods are approximations of the actual calculations. Performance can be further improved if better implementations of SVD which do not sacrifice accuracy for speed are used in calculating the Principal Components.

4.4. Text-to-Image Image Generative Models

We showcase EigenLoRAX’s versatility on complex multimodal tasks like text-to-image generation, where LoRAs are extensively used to adapt models like Stable Diffusion to various styles and datasets. Despite thousands of LoRA adapters being available, most remain underutilized, occupying significant memory alongside their data. As adapter usage grows, a critical challenge is efficiently hosting multiple adapters for diverse tasks, especially on edge devices. Switching adapters during inference, often from CPU memory or disk, introduces latency that hinders real-time applications. EigenLoRAX tackles this by extracting a shared task-invariant subspace, significantly reducing in-memory parameters and enabling memory-efficient inference without compromising flexibility or performance. EigenLoRAX

Table 4: Results for Lots of LoRAs. We report the Rouge-L scores for each of the 5 tasks from the training set and 5 from the testing set. EigenLoRAX achieves on average **88%** of LoRA’s performance while requiring anywhere from $12\times$ to $95\times$ less parameters in a zero-shot setting.

METHOD	# TRAINABLE PARAMETERS	076	627	664	819	1631	039	290	391	442	1598	AVG.
LoRA ($r = 16$)	9.4M	69.05	23.96	25	75	99.04	58.77	93.79	93.45	67.84	51.58	65.75
EIGENLoRAX ^{ZS}	98-786K	60.78	18.91	33.33	65.07	94.74	49.96	84.54	88.56	49.78	39.81	58.25
PERFORMANCE RATIO		0.88	0.79	1.33	0.87	0.96	0.79	0.90	0.95	0.73	0.77	0.88



Figure 4: LoRAs (top) vs. EigenLoRAX (bottom) in Text-to-Image generation. (Left) A single EigenLoRAX analytically reconstructs multiple LoRAs, significantly reducing memory ($18\times$ reduction) and compute costs. (Right) It efficiently learns new tasks with up to $100\times$ fewer parameters than LoRA, maintaining similar visual quality. See Appendix A.3 for more examples.

can effectively replace pretrained adapters, drastically reducing storage requirements. To demonstrate this, we extracted $K = 14$ principal components from $N = 20$ Stable Diffusion-XL (Podell et al., 2023) LoRA adapters (rank $r = 32$) from the HuggingFace diffusers library (von Platen et al., 2022). Using $\alpha \in \mathbb{R}^{r \times K}$, we analytically reconstructed the original LoRA weights within the extracted principal subspace. For image generation, we used 30 denoising steps with a fixed seed of 0. Results and comparisons are shown in Figure 4. This approach reduces storage requirements for all adapters from 4.6GB to just 261MB, achieving an **18 \times reduction in low-rank parameters stored in memory**. By enabling a large number of adapters to reside in VRAM simultaneously, EigenLoRAX eliminates I/O bottlenecks, significantly improving memory efficiency for real-time applications.

Failure Cases and Limitations Despite its advantages, EigenLoRAX has limitations. Figure 5 shows a failure case where the method fails to capture a key property of the desired image. While tasks may share a principal subspace, missing critical orthogonal components can degrade performance, especially if they were absent in the pretrained LoRAs used for extraction or if the chosen top K components were suboptimal. In the latter case, empirical analysis of hyperparameters (Appendix B) can guide optimal K selection. Additionally, our subspace augmentation method (Table 3) helps by iteratively sampling and orthogonalizing more components to recover missing subspace elements. A simple extension can further mitigate this issue by allowing

a small number of rank-1 weights to be trainable outside the subspace. Another key limitation (Section 4.3) is the computational cost and instability of processing a large number of initial LoRAs. A continual learning approach building on our method could address this. Finally, our experiments did not explore layer-wise or weight matrix-level optimizations; we tested different K values but kept them fixed across layers and for both A and B matrices. Additional failure cases are discussed in Appendix B.2.

5. Conclusion

We introduce EigenLoRAX, a PEFT method that recycles trained adapters by finding a shared principal subspace. This allows for more efficient training of new adapters and inference with multiple adapters. Through experiments, we showed that EigenLoRAX works and provides practical benefits in a wide range of scenarios. Our method has the potential to mitigate the perpetually widening compute resource gap (Ahmed & Wahed, 2020; Besiroglu et al., 2024) and reduce the environmental cost of training and using AI models (Wu et al., 2021; Ligozat et al., 2021). It also holds promise for training personalized models (Tan et al., 2024) on low-resource devices, in privacy-critical use-cases. We have a large number of experiments (6+) on a diverse set of complex models, tasks and modalities. We have shown that EigenLoRAX excels in faster and efficient learning, memory savings and zero shot performance which differentiates it from conventional PeFT models. While our work



Figure 5: Failure Case: EigenLoRAX may fail if an important component is missing from the initialized subspace i.e. the shared subspace is incomplete, which may happen due to inadequacy in the number of initial adapters or due to the majority of the adapters being of bad quality. E.g., the model may have lost the essential "mosaic" property when generating an image for the prompt: "mosaic picture of a dog."

is application-focused, we believe it is the first work to hypothesize and empirically prove the existence of shared weight subspaces of neural networks. This important insight has significant implications of model merging, efficiency, mechanistic interpretability, and neural learning theory.

References

Ahmed, N. M. and Wahed, M. The de-democratization of ai: Deep learning and the compute divide in artificial intelligence research. *ArXiv*, abs/2010.15581, 2020. URL <https://api.semanticscholar.org/CorpusID:225102971>.

Angtian, W., Kortylewski, A., and Yuille, A. Nemo: Neural mesh models of contrastive features for robust 3d pose estimation. In *Proceedings International Conference on Learning Representations (ICLR)*, 2021.

Bartlett, P. L. and Mendelson, S. Rademacher and gaussian complexities: risk bounds and structural results. *J. Mach. Learn. Res.*, 3(null):463–482, March 2003. ISSN 1532-4435.

Besiroglu, T., Bergerson, S. A., Michael, A., Heim, L., Luo, X., and Thompson, N. The compute divide in machine learning: A threat to academic contribution and scrutiny? *ArXiv*, abs/2401.02452, 2024. URL <https://api.semanticscholar.org/CorpusID:266818226>.

Bossard, L., Guillaumin, M., and Van Gool, L. Food-101 – mining discriminative components with random forests. In *European Conference on Computer Vision*, 2014.

Brown, T. B., Mann, B., Ryder, N., Subbiah, M., Kaplan, J., Dhariwal, P., Neelakantan, A., Shyam, P., Sastry, G., Askell, A., Agarwal, S., Herbert-Voss, A., Krueger, G., Henighan, T., Child, R., Ramesh, A., Ziegler, D. M., Wu, J., Winter, C., Hesse, C., Chen, M., Sigler, E., Litwin, M., Gray, S., Chess, B., Clark, J., Berner, C., McCandlish, S., Radford, A., Sutskever, I., and Amodei, D. Language models are few-shot learners. In *Proceedings of the 34th International Conference on Neural Information Processing Systems, NIPS '20*, Red Hook, NY, USA, 2020. Curran Associates Inc. ISBN 9781713829546.

Brüel-Gabrielsson, R., Zhu, J., Bhardwaj, O., Choshen, L., Greenwald, K., Yurochkin, M., and Solomon, J. Compress then serve: Serving thousands of lora adapters with little overhead, 2024. URL <https://arxiv.org/abs/2407.00066>.

Burer, S. and Monteiro, R. D. C. A nonlinear programming algorithm for solving semidefinite programs via low-rank factorization. *Mathematical Programming*, 95:329–357, 2003. URL <https://api.semanticscholar.org/CorpusID:7691228>.

Chen, S., Ge, C., Tong, Z., Wang, J., Song, Y., Wang, J., and Luo, P. Adaptformer: Adapting vision transformers for scalable visual recognition. *ArXiv*, abs/2205.13535, 2022. URL <https://api.semanticscholar.org/CorpusID:249097890>.

Chi, Y., Lu, Y. M., and Chen, Y. Nonconvex optimization meets low-rank matrix factorization: An overview. *IEEE Transactions on Signal Processing*, 67(20):5239–5269, 2019. doi: 10.1109/TSP.2019.2937282.

Chughtai, B., Chan, L., and Nanda, N. A toy model of universality: Reverse engineering how networks learn group operations, 2023. URL <https://arxiv.org/abs/2302.03025>.

Diao, S., Xu, T., Xu, R., Wang, J., and Zhang, T. Mixture-of-Domain-Adapters: Decoupling and Injecting Domain Knowledge to Pre-trained Language

Models Memories. June 2023. doi: 10.48550/arXiv.2306.05406.

Dosovitskiy, A., Beyer, L., Kolesnikov, A., Weissenborn, D., Zhai, X., Unterthiner, T., Dehghani, M., Minderer, M., Heigold, G., Gelly, S., Uszkoreit, J., and Houlsby, N. An image is worth 16x16 words: Transformers for image recognition at scale. In *International Conference on Learning Representations*, 2021. URL <https://openreview.net/forum?id=YicbFdNTTy>.

Fischer, M., Bartler, A., and Yang, B. Prompt tuning for parameter-efficient medical image segmentation. *Medical Image Analysis*, 91:103024, 2024.

Gain, A., Kaushik, P., and Siegelmann, H. Adaptive neural connections for sparsity learning. In *Proceedings of the IEEE/CVF Winter Conference on Applications of Computer Vision (WACV)*, March 2020.

Gavish, M. and Donoho, D. L. The optimal hard threshold for singular values is $4/\sqrt{3}$, 2014. URL <https://arxiv.org/abs/1305.5870>.

Guth, F. and Ménard, B. On the universality of neural encodings in CNNs. In *ICLR 2024 Workshop on Representational Alignment*, 2024. URL <https://openreview.net/forum?id=ofEBFOrITI>.

Houlsby, N., Giurgiu, A., Jastrzebski, S., Morrone, B., De Laroussilhe, Q., Gesmundo, A., Attariyan, M., and Gelly, S. Parameter-efficient transfer learning for NLP. In Chaudhuri, K. and Salakhutdinov, R. (eds.), *Proceedings of the 36th International Conference on Machine Learning*, volume 97 of *Proceedings of Machine Learning Research*, pp. 2790–2799. PMLR, 09–15 Jun 2019. URL <https://proceedings.mlr.press/v97/houlsby19a.html>.

Hu, E. J., Shen, Y., Wallis, P., Allen-Zhu, Z., Li, Y., Wang, S., Wang, L., and Chen, W. Lora: Low-rank adaptation of large language models. *arXiv preprint arXiv:2106.09685*, 2021.

Huang, C., Liu, Q., Lin, B. Y., Pang, T., Du, C., and Lin, M. Lorahub: Efficient cross-task generalization via dynamic lora composition. *arXiv preprint arXiv:2307.13269*, 2023.

Jiang, A. Q., Sablayrolles, A., Mensch, A., Bamford, C., Chaplot, D. S., de las Casas, D., Bressand, F., Lengyel, G., Lample, G., Saulnier, L., Lavaud, L. R., Lachaux, M.-A., Stock, P., Scao, T. L., Lavril, T., Wang, T., Lacroix, T., and Sayed, W. E. Mistral 7b, 2023. URL <https://arxiv.org/abs/2310.06825>.

Kaushik, P., Gain, A., Kortylewski, A., and Yuille, A. Understanding catastrophic forgetting and remembering in continual learning with optimal relevance mapping, 2021. URL <https://arxiv.org/abs/2102.11343>.

Kaushik, P., Kortylewski, A., and Yuille, A. A bayesian approach to ood robustness in image classification. In *Proceedings of the IEEE/CVF Conference on Computer Vision and Pattern Recognition (CVPR)*, pp. 22988–22997, June 2024a.

Kaushik, P., Mishra, A., Kortylewski, A., and Yuille, A. L. Source-free and image-only unsupervised domain adaptation for category level object pose estimation. *ArXiv*, abs/2401.10848, 2024b. URL <https://api.semanticscholar.org/CorpusID:267060973>.

Koohpayegani, S. A., L, N. K., Nooralinejad, P., Kolouri, S., and Pirsavash, H. NOLA: Compressing loRA using linear combination of random basis. In *The Twelfth International Conference on Learning Representations*, 2024. URL <https://openreview.net/forum?id=TjfxCdgvzk>.

Kopitzko, D. J., Blankevoort, T., and Asano, Y. M. VeRA: Vector-based Random Matrix Adaptation. October 2023. URL <https://openreview.net/forum?id=NjNfLdxr3A>.

Krizhevsky, A., Nair, V., and Hinton, G. Cifar-100 (canadian institute for advanced research). 2009. URL <http://www.cs.toronto.edu/~kriz/cifar.html>.

Ku, L.-W., Martins, A., and Srikumar, V. (eds.). *Proceedings of the 62nd Annual Meeting of the Association for Computational Linguistics (Volume 1: Long Papers)*, Bangkok, Thailand, August 2024. Association for Computational Linguistics. URL <https://aclanthology.org/2024.acl-long.0>.

Kwon, S. M., Zhang, Z., Song, D., Balzano, L., and Qu, Q. Efficient compression of overparameterized deep models through low-dimensional learning dynamics, 2024. URL <https://arxiv.org/abs/2311.05061>.

Lester, B., Al-Rfou, R., and Constant, N. The power of scale for parameter-efficient prompt tuning. In Moens, M.-F., Huang, X., Specia, L., and Yih, S. W.-t. (eds.), *Proceedings of the 2021 Conference on Empirical Methods in Natural Language Processing*, pp. 3045–3059, Online and Punta Cana, Dominican Republic, November 2021. Association for Computational Linguistics. doi: 10.18653/v1/2021.emnlp-main.243. URL <https://aclanthology.org/2021.emnlp-main.243>.

Ligozat, A.-L., Lefèvre, J., Bugeau, A., and Combaz, J. Unraveling the hidden environmental impacts of ai solutions for environment. *ArXiv*, abs/2110.11822, 2021. URL <https://api.semanticscholar.org/CorpusID:239616423>.

Liu, D., Kong, H., Luo, X., Liu, W., and Subramanian, R. Bringing ai to edge: From deep learning's perspective. *Neurocomput.*, 485(C):297–320, May 2022. ISSN 0925-2312. doi: 10.1016/j.neucom.2021.04.141. URL <https://doi.org/10.1016/j.neucom.2021.04.141>.

Liu, S.-Y., Wang, C.-Y., Yin, H., Molchanov, P., Wang, Y.-C. F., Cheng, K.-T., and Chen, M.-H. Dora: Weight-decomposed low-rank adaptation, 2024. URL <https://arxiv.org/abs/2402.09353>.

Liu, Y., Ott, M., Goyal, N., Du, J., Joshi, M., Chen, D., Levy, O., Lewis, M., Zettlemoyer, L., and Stoyanov, V. Roberta: A robustly optimized bert pretraining approach. *ArXiv*, abs/1907.11692, 2019. URL <https://api.semanticscholar.org/CorpusID:198953378>.

Luo, G., Huang, M., Zhou, Y., Sun, X., Jiang, G., Wang, Z., and Ji, R. Towards efficient visual adaption via structural re-parameterization. *arXiv preprint arXiv:2302.08106*, 2023.

Ma, C., Xu, X., Tong, T., and Chi, Y. *Provably Accelerating Ill-Conditioned Low-Rank Estimation via Scaled Gradient Descent, Even with Overparameterization*, pp. 133–165. Springer Nature Switzerland, Cham, 2024. ISBN 978-3-031-66497-7. doi: 10.1007/978-3-031-66497-7_7. URL https://doi.org/10.1007/978-3-031-66497-7_7.

Mangrulkar, S., Gugger, S., Debut, L., Belkada, Y., Paul, S., and Bossan, B. Peft: State-of-the-art parameter-efficient fine-tuning methods. <https://github.com/huggingface/peft>, 2022.

Meng, F., Wang, Z., and Zhang, M. PiSSA: Principal Singular Values and Singular Vectors Adaptation of Large Language Models, May 2024. URL <https://arxiv.org/abs/2404.02948>. arXiv:2404.02948 [cs].

Nilsback, M.-E. and Zisserman, A. Automated flower classification over a large number of classes. In *Indian Conference on Computer Vision, Graphics and Image Processing*, Dec 2008.

Podell, D., English, Z., Lacey, K., Blattmann, A., Dockhorn, T., Müller, J., Penna, J., and Rombach, R. Sdxl: Improving latent diffusion models for high-resolution image synthesis, 2023. URL <https://arxiv.org/abs/2307.01952>.

Razdaibiedina, A., Mao, Y., Khabsa, M., Lewis, M., Hou, R., Ba, J., and Almahairi, A. Residual prompt tuning: improving prompt tuning with residual reparameterization. In Rogers, A., Boyd-Graber, J., and Okazaki, N. (eds.), *Findings of the Association for Computational Linguistics: ACL 2023*, pp. 6740–6757, Toronto, Canada, July 2023. Association for Computational Linguistics. doi: 10.18653/v1/2023.findings-acl.421. URL <https://aclanthology.org/2023.findings-acl.421>.

Rombach, R., Blattmann, A., Lorenz, D., Esser, P., and Ommer, B. High-resolution image synthesis with latent diffusion models. *2022 IEEE/CVF Conference on Computer Vision and Pattern Recognition (CVPR)*, pp. 10674–10685, 2021. URL <https://api.semanticscholar.org/CorpusID:245335280>.

Sharma, P., Ash, J. T., and Misra, D. The Truth is in There: Improving Reasoning in Language Models with Layer-Selective Rank Reduction, December 2023. URL <https://arxiv.org/abs/2312.13558>. arXiv:2312.13558 [cs].

Shenaj, D., Toldo, M., Rigon, A., and Zanuttigh, P. Asynchronous federated continual learning. *2023 IEEE/CVF Conference on Computer Vision and Pattern Recognition Workshops (CVPRW)*, pp. 5055–5063, 2023. URL <https://api.semanticscholar.org/CorpusID:258041245>.

Sun, Q., Cetin, E., and Tang, Y. Transformer-squared: Self-adaptive llms, 2025. URL <https://arxiv.org/abs/2501.06252>.

Tan, Z., Zeng, Q., Tian, Y., Liu, Z., Yin, B., and Jiang, M. Democratizing large language models via personalized parameter-efficient fine-tuning. *arXiv preprint arXiv:2402.04401*, 2024.

Touvron, H., Lavril, T., Izacard, G., Martinet, X., Lachaux, M.-A., Lacroix, T., Rozière, B., Goyal, N., Hambro, E., Azhar, F., Rodriguez, A., Joulin, A., Grave, E., and Lample, G. Llama: Open and efficient foundation language models. *ArXiv*, abs/2302.13971, 2023. URL <https://api.semanticscholar.org/CorpusID:257219404>.

von Platen, P., Patil, S., Lozhkov, A., Cuenca, P., Lambert, N., Rasul, K., Davaadorj, M., Nair, D., Paul, S., Berman, W., Xu, Y., Liu, S., and Wolf, T. Diffusers: State-of-the-art diffusion models. <https://github.com/huggingface/diffusers>, 2022.

Wang, A., Singh, A., Michael, J., Hill, F., Levy, O., and Bowman, S. R. Glue: A multi-task benchmark and anal-

ysis platform for natural language understanding, 2019.
 URL <https://arxiv.org/abs/1804.07461>.

Wang, Y., Mishra, S., Alipoormolabashi, P., Kordi, Y., Mirzaei, A., Naik, A., Ashok, A., Dhanasekaran, A. S., Arunkumar, A., Stap, D., Pathak, E., Karamanolakis, G., Lai, H., Purohit, I., Mondal, I., Anderson, J., Kuznia, K., Doshi, K., Pal, K. K., Patel, M., Moradshahi, M., Parmar, M., Purohit, M., Varshney, N., Kaza, P. R., Verma, P., Puri, R. S., Karia, R., Doshi, S., Sampat, S. K., Mishra, S., Reddy A, S., Patro, S., Dixit, T., and Shen, X. Super-NaturalInstructions: Generalization via declarative instructions on 1600+ NLP tasks. In Goldberg, Y., Kozareva, Z., and Zhang, Y. (eds.), *Proceedings of the 2022 Conference on Empirical Methods in Natural Language Processing*, pp. 5085–5109, Abu Dhabi, United Arab Emirates, December 2022. Association for Computational Linguistics. doi: 10.18653/v1/2022.emnlp-main.340. URL [https://aclanthology.org/2022.emnlp-main.340/](https://aclanthology.org/2022.emnlp-main.340).

Wu, C.-J., Raghavendra, R., Gupta, U., Acun, B., Ardalani, N., Maeng, K., Chang, G., Behram, F. A., Huang, J., Bai, C., Gschwind, M. K., Gupta, A., Ott, M., Melnikov, A., Candido, S., Brooks, D., Chauhan, G., Lee, B., Lee, H.-H. S., Akyildiz, B., Balandat, M., Spisak, J., Jain, R. K., Rabbat, M. G., and Hazelwood, K. M. Sustainable ai: Environmental implications, challenges and opportunities. *ArXiv*, abs/2111.00364, 2021. URL <https://api.semanticscholar.org/CorpusID:240354766>.

Wu, X., Huang, S., and Wei, F. Mixture of lora experts. *arXiv preprint arXiv:2404.13628*, 2024.

Zhang, Q., Chen, M., Bukharin, A., Karampatziakis, N., He, P., Cheng, Y., Chen, W., and Zhao, T. Adalora: Adaptive budget allocation for parameter-efficient fine-tuning, 2023. URL <https://arxiv.org/abs/2303.10512>.

Zhong, M., Shen, Y., Wang, S., Lu, Y., Jiao, Y., Ouyang, S., Yu, D., Han, J., and Chen, W. Multi-lora composition for image generation. *arXiv preprint arXiv:2402.16843*, 2024.

Zhou, Q., Zheng, K., Hou, L., Xing, J., and Xu, R. X-lora: An open source lpwa network. *arXiv preprint arXiv:1812.09012*, 2018.

Zhou, Y., Lei, T., Liu, H., Du, N., Huang, Y., Zhao, V. Y., Dai, A. M., Chen, Z., Le, Q. V., and Laudon, J. Mixture-of-experts with expert choice routing. In Oh, A. H., Agarwal, A., Belgrave, D., and Cho, K. (eds.), *Advances in Neural Information Processing Systems*, 2022. URL <https://openreview.net/forum?id=jdJ01HIVinI>.

Zoph, B., Bello, I., Kumar, S., Du, N., Huang, Y., Dean, J., Shazeer, N., and Fedus, W. St-moe: Designing stable and transferable sparse expert models, 2022. URL <https://arxiv.org/abs/2202.08906>.

A. Appendix

A.1. Experiments

For VeRA, LoRA and PiSSA, we experimented with a range of learning rates, from higher to lower, along with three different scheduling approaches: ReduceLRonPlateau, Linear, and Cosine. The hyperparameters that yielded the best average performance were selected for further experimentation. The observed discrepancies with EigenLoRAX hyperparameters are attributable to these methodological choices. Comprehensive hyperparameter tuning for EigenLoRAX was not pursued extensively, as the initially selected hyperparameters, notably a high learning rate paired with ReduceLRonPlateau or Linear, demonstrated satisfactory performance, thereby conserving computational resources.

A.1.1. IMAGE CLASSIFICATION

Trainable parameters for EigenLoRAX The base model is vit-base-patch16-224. The following are the trainable parameters in ViT (Dosovitskiy et al., 2021) that are trained for EigenLoRAX. We ignore the last linear layer for simplicity since it is trained for all models and baselines and is constant. The loading parameter has the shape of [number of EigenLoRAX PC, 1] (we only have 2 in each EigenLoRAX PC for this experiment). Therefore, the total number of trainable parameters (for the number of components= 2) is 12 (layers) \times 4 (set of parameters per layers) \times 2 (number of trainable parameter per coefficient) = 96 trainable parameters.

Hyperparameters LoRA (Hu et al., 2021) and VeRA (Kopczko et al., 2023) implementations are taken from the HuggingFace PEFT (Mangrulkar et al., 2022) library with hyperparameters of the default method. For Food101 (Bossard et al., 2014) experiment, we randomly remove 1 class for ease of compute. Experimental hyperparameters are reported in Table 5 and Table 6.

Table 5: Hyperparameters for LoRA (Hu et al., 2021) and VeRA (Kopczko et al., 2023) for the Image Classification Experiment

	CIFAR100	Flowers102	Food101
Learning Rate	1e-4	1e-4	1e-4
Weight Decay	0.1	0.1	0.1
Warmup ratio	0.06	0.06	0.06
Epochs	10	10	10
Number of Subsets	5	6	5
Categories/Subset	20	17	20
Seed	42	42	42
Batch Size	128	64	128

Table 6: Hyperparameters for EigenLoRAX for the Image Classification Experiment

	CIFAR100	Flowers102	Food101
Learning Rate	1e-2	1e-2	1e-2
Weight Decay	0.1	0.1	0.1
Warmup ratio	0.06	0.06	0.06
Epochs	10	10	10
Number of Subsets	5	6	5
Categories/Subset	20	17	20
Seed	42	42	42
Batch Size	128	64	128

Experimental Results The experiments were conducted 5 times utilizing randomly generated dataset splits. The mean accuracy values are reported in Table 1. Empirical analysis indicates that without control and annealing of learning rates, the

loss for both LoRA and VeRA may diverge or plateau, particularly with high learning rates. Even with the lower learning rate, Full training or LoRA can overfit to the training data without proper regularization. In contrast, no such instability was observed during EigenLoRAX training, where a relatively higher learning rate proved advantageous for rapid convergence.

Table 7: Image Classification Accuracy results on CIFAR100 (Krizhevsky et al., 2009)

Model	Trainable	subset1	subset2	subset3	subset4	subset5	Avg.
	Params						
FT	86389248	98.8	97.95	95.55	96.05	96.3	96.93
LoRA ($r = 1$)	36864	97.6	93.95	93.75	91.75	85.2	92.45
LoRA ($r = 4$)	147456	98.15	95.2	93.5	92.85	89.25	93.79
VeRA ($r = 2$)	18480	93.65	89.7	89.5	89.95	91.55	90.87
EigenLoRAX ($K = 2$)	96	97.25	95.05	94.55	93	94.15	94.8

Table 8: Image Classification Accuracy results on Food101 (Bossard et al., 2014)

Model	Trainable	subset1	subset2	subset3	subset4	subset5	Avg.
	Params						
FT	86389248	98.64	97	97.36	94.28	95.92	96.64
LoRA ($r = 1$)	36864	93.36	88.44	94.28	89.4	89.9	91.076
LoRA ($r = 4$)	147456	98.2	96.96	96.08	92.88	94.52	95.728
VeRA ($r = 2$)	18480	91.22	88.42	94.42	91.88	92.82	91.752
EigenLoRAX ($K = 2$)	96	97.24	95.96	96	91.88	94.6	95.136

Table 9: Image Classification Accuracy results on Flowers102 (Nilsback & Zisserman, 2008)

Model	subset1	subset2	subset3	subset4	subset5	subset6	Avg.
FT	99.7	99.3	98.01	98.22	99.7	98.01	98.82
LoRA ($r = 1$)	85.9	88.47	92.69	91.02	91.7	91.01	90.13
LoRA ($r = 4$)	96.23	92.76	97.22	95.01	98.24	90.73	95.03
VeRA ($r = 2$)	99.2	95.4	97.7	94.7	90.9	95	95.48
EigenLoRAX ($K = 2$)	99.686	97.905	97.689	98.291	99.344	97.718	98.43

A.2. Natural Language Processing - GLUE benchmark

Hyperparameters LoRA (Hu et al., 2021), VeRA (Kopitzko et al., 2023) and PISSA (Meng et al., 2024) implementations are taken from the HuggingFace PEFT (Mangrulkar et al., 2022) library. Refer to Table 10 and Table 11 for hyperparameter details. For LoRA (Hu et al., 2021), we use the ranks $\in \{8, 16\}$. For VeRA (Kopitzko et al., 2023), we use rank= 256, and for EigenLoRAX, we use $K \in \{16, 32\}$ and $r = 8$. Here, r refers to the dimensionality of the trainable coefficients and not the rank. For both PISSA (Meng et al., 2024) and LoRA, all the parameters of the low rank matrix are trainable. For the EigenLoRAX initialization experiment, we train both the components and coefficients for a fair comparison with PISSA. In practice, however, we do not need to do so - we can tune only the sparse coefficients and after the loss converges, finetune the components for a few training steps.

Table 10: Hyperparameters for LoRA (Hu et al., 2021), VeRA (Kopitzko et al., 2023) and PiSSA (Meng et al., 2024) for the GLUE benchmark. (Wang et al., 2019)

	CoLA	MRPC	QNLI	RTE	SST-2	STSB
Learning Rate	4e-4	4e-4	4e-4	5e-4	5e-4	4e-4
Weight Decay	0.1	0.1	0.1	0.1	0.1	0.1
Warmup ratio	0.06	0.06	0.06	0.06	0.06	0.06
Epochs	80	30	25	80	60	40
Scheduler	Linear	Linear	Linear	Linear	Linear	Linear
Seed	0	0	0	0	0	0
Batch Size	64	64	64	64	64	64

Table 11: Hyperparameters for EigenLoRAX for the GLUE benchmark. (Wang et al., 2019).
(RLrP - ReduceLRonPlateau)

	CoLA	MRPC	QNLI	RTE	SST-2	STSB
Learning Rate	4e-3	4e-3	4e-3	5e-3	5e-3	4e-3
Weight Decay	0.1	0.1	0.1	0.1	0.1	0.1
Warmup ratio	0.06	0.06	0.06	0.06	0.06	0.06
Epochs	80	30	25	80	60	40
Scheduler	RLrP	RLrP	RLrP	RLrP	RLrP	RLrP
Seed	0	0	0	0	0	0
Batch Size	64	64	64	64	64	64

A.3. Text-to-Image Generation (Stable Diffusion Models)

Figure 6 and Figure 7 show more examples of a text-to-image stable diffusion model finetuned using EigenLoRAX. Note that not only there is no publicly available code for VeRA that allows its usage in complex text-to-image generation tasks, but our VeRA implementation also did not work well in this task.

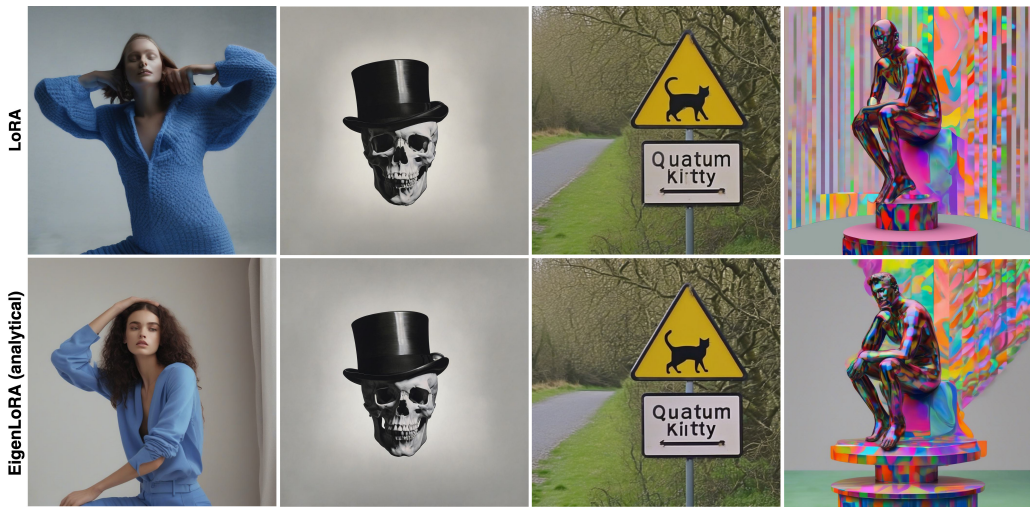


Figure 6: (Part 1) A single EigenLoRAx (identical components, varying loadings) was employed to produce these images utilizing the Stable Diffusion-XL (Podell et al., 2023) model. A comparison between our results and those obtained from multiple LoRAs does not show a noticeable degradation in visual quality.



Figure 7: (Part 2) A single EigenLoRAx (identical components, varying loadings) was employed to produce these images utilizing the Stable Diffusion-XL (Podell et al., 2023) model. A comparison between our results and those obtained from multiple LoRAs demonstrates no noticeable degradation in visual quality.



Figure 8: Analytical reconstruction of LoRAs using EigenLoRAX which shows no degradation in relative visual quality. See Appendix A.3 for more examples.



Figure 9: Comparison of generated images by LoRA and EigenLoRAX trained on Torino Aqua anime style images. For EigenLoRAX, we utilized 12 components with only trainable coefficients to finetune the base model.

A.4. Additional Experiments

Furthermore, we also performed a 3D object pose estimation (Angtian et al., 2021; Kaushik et al., 2024b) finetuning experiment using a modified Resnet-101. The task of 3D object pose estimation involves the prediction of three rotation parameters (azimuth, elevation, in-plane rotation) of an object relative to the camera. The pose estimation error between the predicted rotation matrix and the ground truth rotation matrix is given as $\Delta(R_{pred}, R_{gt}) = \frac{\|\log_b(R_{pred}^T R_{gt})\|_F}{\sqrt{2}}$. We show the results for the $\frac{\pi}{6}$ accuracy threshold for this experiment.

Table 12: 3D object pose estimation accuracy ($\frac{\pi}{6}$ threshold)

Method	Param	Airplane	Motorbike	Boat	Bottle	Bus	Car	Average
LoRA ($r = 16$)	215K	79.9	80.1	71.5	89.8	90.1	96.6	84.67
VeRA ($r = 256$)	40K	68.4	72.4	64.3	88.4	87.2	94.4	79.18
EigenLoRAX ($K = 2$)	16K	81.4	80.0	71.4	90	92.3	97.5	85.43

B. Method Analysis and Ablation

Through a rigorous comparative analysis of EigenLoRAXs and their target LoRAs, we identified that the most pronounced reconstruction discrepancies manifest in the initial and terminal layers of the neural network, as depicted in Figure 10. Allowing the EigenLoRAX PCs in these layers to undergo fine-tuning alongwith the coefficients can alleviate failure scenarios, thereby alleviating the need for comprehensive model fine-tuning.

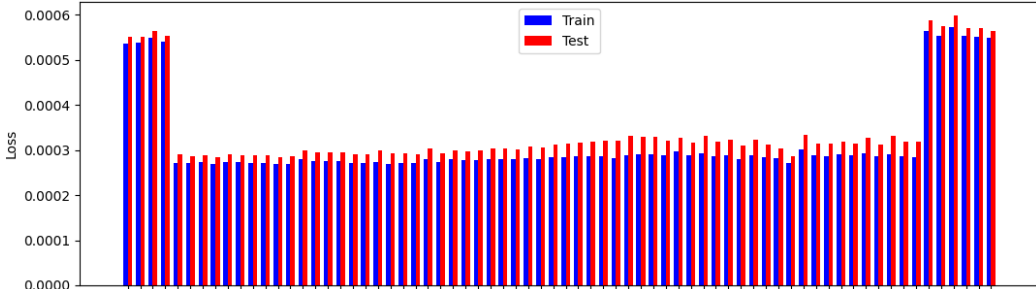


Figure 10: Average reconstruction error between EigenLoRAX and a set of LoRAs for all UNet layers in a stable diffusion model.

B.1. How to Choose K Principal Components and r for EigenLoRAX

We perform an ablation study on the selection of EigenLoRAX principal components (K). Our analysis concentrates on one experiment as shown in Figure 13, specifically pertaining to the MRPC task within the GLUE (Wang et al., 2019) benchmark. The analysis in Figure 11 shows the training loss in relation to increasing number of EigenLoRAX principal components K , as well as the explained variance of the LoRAs used to initialize the EigenLoRAX in Figure 12. We find, empirically, that choosing EigenLoRAX PCs for the explained variance of 50 – 80% of the LoRAs used to initialize EigenLoRAX is sufficient for a robust initialization. This is shown in Figure 12 where we choose $K = 8$ which roughly corresponds to the explained variance of 55 – 60%. We further ablate this choice in Figure 11, where although substantial improvements are evident up to $K = 8$, an increase in the number of K thereafter yields only marginal gains, demonstrating diminishing returns as the number of components increases. The parameter r in EigenLoRAX does not equate the *rank* parameter in LoRA and its variants. It reflects the dimensionality of the EigenLoRAX coefficients. Although $r = 1$ works well, we observe slight performance improvements as we increase this value as shown in Figure 14. Increasing this value corresponds to a small amount of parameter increase. We observe no finetuning instability by changing this value and recommend that it can be set to anywhere between 1 and the rank of the LoRAs used to initialize EigenLoRAX.



Figure 11: Training Loss Convergence for different numbers of EigenLoRAX PCs

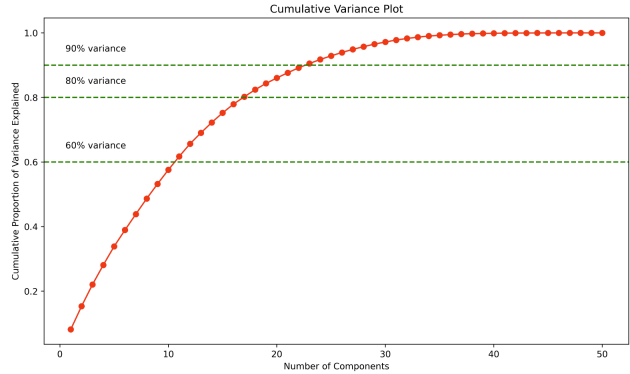


Figure 12: Explained Variance for increasing number of PCs

Figure 13: Ablation of Number of EigenLoRAX Principal Components

B.2. Failure Cases

Figure 5 illustrates a potential failure case of EigenLoRAX, where the incorrect number of principal components (PCs) was selected. In this instance, the "mosaic style" information was excluded from the principal subspace identified by EigenLoRAX due to an insufficient number of PCs. However, this issue can be resolved by selecting a larger number of PCs, as the extended principal subspace contains the necessary information for the task.

Another hypothetical failure scenario arises if the domain gap between the low-rank adapters used to initialize EigenLoRAX and the downstream task is significantly large. Although we do not observe such a case in our experiments, it is plausible that under such conditions, EigenLoRAX might underperform. This issue could potentially be mitigated by allowing only a subset of PCs to remain trainable, enabling the model to adapt more effectively to the target domain.

A further observed limitation of EigenLoRAX occurs in complex tasks like Text-to-Image generation, which may extend to other tasks as well. If the majority of LoRAs used to initialize EigenLoRAX encode biases (e.g., related to gender, race, or context), these biases tend to propagate into EigenLoRAX outputs. While such biases are a common issue in deep learning models trained using stochastic gradient descent or similar methods, addressing them remains a critical area of future work. We consider this an important avenue for improvement and discuss the broader implications in Appendix C.

B.3. Impact of LoRA adapter quality on EigenLoRAX PC initialization

To evaluate EigenLoRAX's robustness to adapter quality and its resistance to noise, we conducted an ablation study on a subset of tasks of the NLU experiment specified in Section 4.2. Specifically, we generated EigenLoRAX adapters using LoRA matrices with varying levels of random noise added. The results are shown in Table 13

Table 13: EigenLoRAX performance on subset of GLUE task using noisy LoRA adapters for initialization

Noise Level	CoLA	MRPC	RTE	STS-B	Avg
5%	60.51	85.45	74.73	89.9	77.65
15%	57.53	83.09	72.92	89.9	75.86
30%	55.23	76.47	71.84	89.8	73.34

The results show that EigenLoRAX exhibits only minor performance changes even as noise levels increase significantly, indicating some robustness to adapter quality. This suggests that EigenLoRAX can still perform effectively without high quality adapters. However, there is a limit to this robustness. If the signal-to-noise ratio (SNR) in the initial LoRA matrices becomes extremely low—where the LoRAs primarily encode noise rather than meaningful information—the effectiveness of EigenLoRAX diminishes. In such cases, the principal components (PCs) extracted by EigenLoRAX would correspond to random directions in the parameter space. Consequently, EigenLoRAX's performance would resemble that of random matrix methods, such as VeRA and NoLA. These methods rely on a large number of random components or bases to

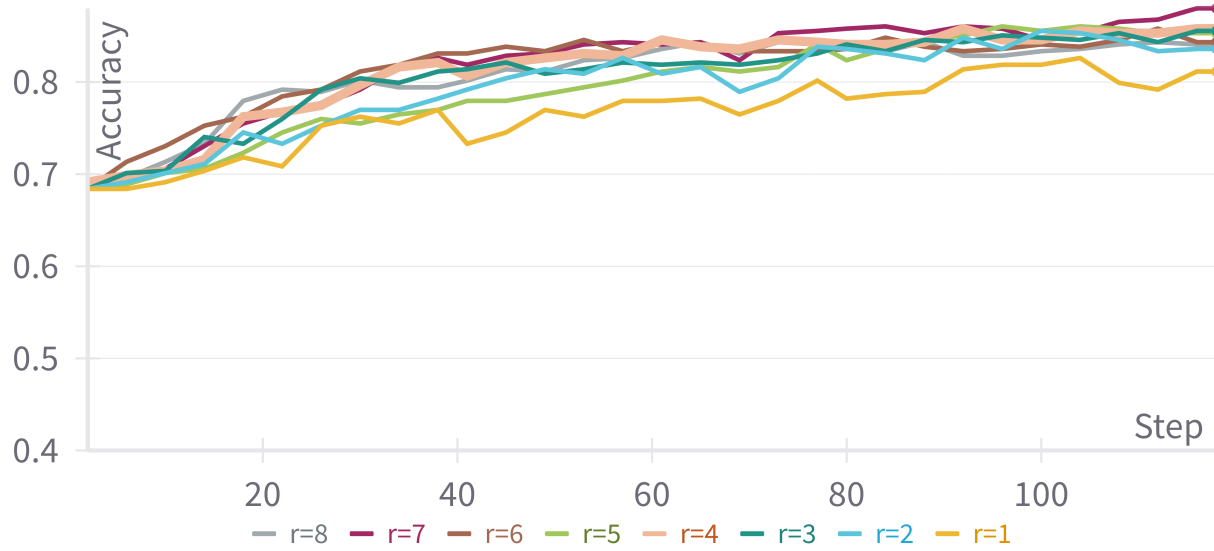


Figure 14: Ablation for the EigenLoRAX’s r hyperparameter. This experiment was done for the MRPC task in the GLUE benchmark.

approximate meaningful results. While they can achieve reasonable performance, they require fine-tuning a substantially larger number of weights associated with these large number of random components, leading to less efficient learning compared to EigenLoRAX. This highlights an important consideration: for EigenLoRAX to maintain its efficiency and effectiveness, the initial LoRA matrices must contain at least a minimal level of meaningful signal. This requirement ensures that EigenLoRAX can leverage the structured information encoded in the LoRAs while avoiding the inefficiencies of purely random approaches.

B.4. Forward pass and backward pass FLOPs

While it is obvious that EigenLoRAX utilized significantly less number of model parameters as the number of tasks in a domain increase, we show that even in terms of floating point operations on a single task, EigenLoRAX is more efficient than LoRA for our experiments. Even for a single task, the number of floating point operations or multiply-accumulate operations in a forward pass for EigenLoRAX is lower than LoRA for all our experiments. Here are the comparisons of the floating point operations (FLOPs) for the forward (fwd FLOPs) and including backward pass (fwd+bwd FLOPs) for each of the Image Classification and GLUE benchmark (batch size = 1) (MFLOPs - MegaFlops):

Table 14: Floating Point Operation calculations for GLUE Benchmark experiment

Method	Training Parameters	fwd FLOPs	fwd+bwd FLOPs
LoRA	1.2M	97,930 MFLOPS	293,800 MFLOPS
VeRA	25K	106,390 MFLOPS	319,170 MFLOPS
EigenLoRAX	12K	97,030 MFLOPS	291,080 MFLOPS

Table 15: Floating Point Operation calculations for Image Classification experiment

Method	Training Parameters	fwd FLOPs	fwd+bwd FLOPs
LoRA	36K	33,773.8 MFLOPS	101,322 MFLOPS
VeRA	18K	33,744.8 MFLOPS	101,234 MFLOPS
EigenLoRAX	96	33,730.2 MFLOPS	101,191 MFLOPS

C. Broader Impact and Implications

This work presents a novel parameter-efficient method for deep learning methods utilizing open source, pretrained Low-Rank Adaptation (LoRA) models. By substantially reducing the computational and memory demands of training and inference, our approach creates a more sustainable and environmentally friendly deep learning paradigm. Our method democratizes accessibility to larger models, making them accessible to researchers and practitioners with limited resources. Furthermore, by harnessing pretrained models, our method can accelerate development and diminish the need for extensive data collection. However, we recognize the inherent risks associated with the use of pretrained models. These include potential biases (racial, gender, etc.), explicit content, since there is no guarantee of the data or method used in training the model, and the potential presence of malicious code. Appropriate caution is advised when using unverified, open-source models.